analytical chemistry

Article

pubs.acs.org/ac

Argon Cluster Ion Source Evaluation on Lipid Standards and Rat Brain Tissue Samples

Claudia Bich,[†] Rasmus Havelund,[‡] Rudolf Moellers,[§] David Touboul,[†] Felix Kollmer,[§] Ewald Niehuis,[§] Ian S. Gilmore,[‡] and Alain Brunelle*[,†]

[†]Centre de Recherche de Gif, Institut de Chimie des Substances Naturelles, CNRS, Avenue de la Terrasse, 91198 Gif-sur-Yvette, France

[‡]Surface and Nanoanalysis, National Physical Laboratory (NPL) Teddington, Middlesex, TW11 0LW, United Kingdom

[§]ION-TOF GmbH, Heisenbergstr.15, 48149 Münster, Germany

Supporting Information

ABSTRACT: Argon cluster ion sources for sputtering and secondary ion mass spectrometry use projectiles consisting of several hundreds of atoms, accelerated to 10−20 keV, and deposit their kinetic energy within the top few nanometers of the surface. For organic materials, the sputtering yield is high removing material to similar depth. Consequently, the exposed new surface is relatively damage free. It has thus been demonstrated on model samples that it is now really possible to perform dual beam depth profiling experiments in organic materials with this new kind of ion source. Here, this possibility has been tested directly on tissue samples, 14 μm thick rat brain sections, allowing primary ion doses much larger than the so-called static secondary ion mass spectrometry (SIMS) limit and demonstrating the possibility to enhance the sensitivity of time-of-flight (TOF)-SIMS biological imaging. However, the depth analyses have also shown some variations of the chemical composition as a function of depth, particularly for cholesterol, as well as some possible matrix effects due to the presence or absence of this compound.

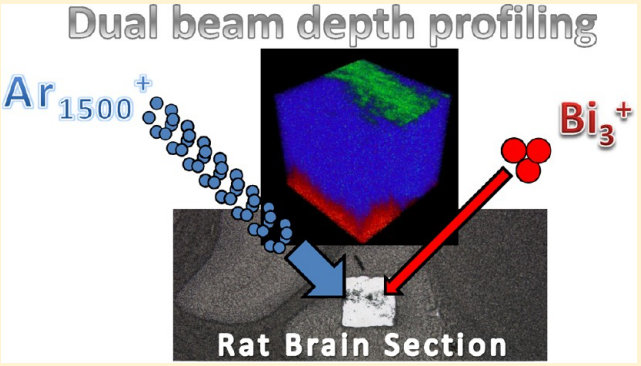

Since the advent of the use of cluster or polyatomic ion sources, like those of gold, bismuth, or fullerenes,[1−4] for the analysis of biological surfaces, cluster-TOF-SIMS (time-of-flight secondary ion mass spectrometry) is becoming a method of choice for mass spectrometry imaging with a lateral resolution in the range of 1 μm or less. However, this analysis method remains a surface analysis one, with subsequent advantages and drawbacks. It is well-known that, in the so-called static-SIMS regime, for which the probability is negligible or very small for an incident primary ion to hit an area which has already been damaged by the impact of a previous projectile, the secondary ion species mostly originate from the first layers within a depth of less than 10 nm.[5] Even if the enhancement of secondary ion emission induced by the replacement of monatomic primary ions by polyatomic ones is taken into account,[1−3,6,7] the number of secondary ions still remains limited in this regime, with secondary ion yields in the 10^{-4} range or below. As pointed out by Fletcher and Vickerman in a recent review,[8] it is simply not possible with only primary ion species like bismuth cluster or any other to overcome the limitation due to the static SIMS regime. The same authors illustrated their demonstration by showing that the intensity scale of lipid images are generally limited to less than 10 counts for a pixel size of around 1−2 μm. Above the static SIMS limit, which is generally admitted to range between several 10^{12} or up to 10^{13} primary ions per square centimeter,[9] the induced damages in organic surfaces like tissue samples become too severe and one can observe a dramatic decrease of the molecular secondary ion yields.

A practical way to increase the sensitivity of TOF-SIMS for biological applications would be to overcome this static SIMS limit and access material beneath the surface. This is done using an increased ion dose to sputter away layers of material which may be analyzed. Unfortunately, the liquid metal ion sources, such as bismuth which are excellent for analytical ion beams owing to high-spatial resolution and high sensitivity create subsurface damage, and so overtime, the signal intensity degrades with a rate depending on the material.[10] A popular configuration for TOF-SIMS instruments is the so-called dual-beam mode where a second ion beam is used to sputter away the material. This conveniently allows the primary beam for analysis and the secondary beam for sputtering to be optimized independently.

Recent studies have shown that argon cluster ion beams are excellent for sputtering organic materials owing to the low

Received: April 6, 2013
Accepted: July 22, 2013
Published: July 22, 2013

energy per atom, typically a few eV per atom, meaning that there is little penetration of argon atoms into the material and also high sputtering yield volumes so that any damage created by the argon atoms is sputtered away leaving a fresh undamaged surface.[11−14] Argon cluster beams are also very efficient to desorb and ionize with high yield large organic molecules like DNA deposited on graphite surface or proteins and more generally to increase the sensitivity of surface deposited compounds.[15−18] Argon is also inert and does not suffer from problems of deposition as is the case for C_{60} projectiles at low energy.[19,20] This allows argon clusters with low total beam energies (a few keV) to achieve superior depth resolution. For example, Shard and co-workers published the results of an interlaboratory study, for which the model sample was made of organic multilayers consisting of ∼400 nm-thick Irganox 1010 matrix with ∼1 nm marker layers of Irganox 3114 at depths of ∼50, 100, 200, and 300 nm. Their results illustrate the great superiority of the argon cluster beams compared to fullerenes.[21] In another study, Wehbe and co-workers compared argon clusters to fullerenes and to low energy cesium beams, using amino-acid stacks as a model sample.[22] Their results also demonstrated the overwhelming advantage of the use of large argon cluster beams. In both studies, the in-depth damage is greatly reduced and the best depth resolution is always obtained with the argon cluster beam.

Large cluster ion beams are therefore well-optimized for sputtering organic materials and can be used in conjunction with a Bi_3 liquid metal ion source for high-spatial resolution imaging and analysis. This is called a two beams or dual beam method. The sequence with analysis using beam-1 and sputtering using beam-2 may be arranged in different patterns. Two common patterns are the so-called interlaced mode where a single short pulse of beam-1 is followed by a longer pulse of beam-2 during the time the secondary ions are traveling through the mass spectrometer. This cycle is typically 10^{-4} s and is usually one pixel in an image scan. An alternative approach is to acquire one full image using beam-1, a single scan, and subsequently sputter for some period of time with beam-2. There are merits of each approach and in the following we use the latter. In principle, beam-2 may be used to sputter or clean away the damage material left by beam-1 in the analysis scan. Consequently, fresh material may be analyzed again by beam-1 with the process repeating until all the material is consumed. It thus enables, layer after layer, action as if going beyond the static SIMS limit, like in the pioneering work published by Tempez and co-workers some years ago with large gold clusters (Au_{400}^{4+}).[23] There are some important aspects about this: (1) Assuming beam-1 causes significant signal loss through molecular damage, the maximum gain in signal intensity that may be achieved by summing intensity as material is consumed is approximately equal to the ratio of the tissue thickness to the damage depth caused by beam-1. Calculations by SRIM[24] show that an 8.3 keV Bi projectile impacting a biological material (Mammary Gland) at 45 degrees has a range of 14.9 nm, and experimental measurements by Muramoto et al.[25] of the implantation depth for Bi_n^+ into tetraglyme and trehalose show similar values and excellent agreement with TRIM calculations.[19] A value of twice this, for safety, could be used to define the damage depth. Therefore, for an analyte uniformly distributed in a 10 μm thick tissue sample, an increase in sensitivity of approximately 330 times is possible. Analytically, this is comparable to the situation with MALDI where the matrix transports analyte from a volume of similar dimensions in the tissue to the ablation volume. (2) 3D images may be reconstructed from the data but, of course, need to be realigned since for a 45° angle of incidence for every micrometer of sputtered depth the image shifts one micrometer toward beam-1.

It should be noted that 3D imaging with a single beam arrangement has important advantages, not least the simplification in instrumentation. The difficulty at present is that it is not possible to focus large cluster sources suitable for organic depth profiling, such as C_{60} and Ar clusters, to better than around 10 μm without severely reducing the beam current and consequently requiring unacceptably long acquisition times. Another limitation of a single beam arrangement is that C_{60} or Argon cluster ion beams are difficult to be simultaneously focused to 1−2 μm and bunched to short pulses, which is mandatory in a time-of-flight analyzer to maintain a high mass resolution, while maintaining currents high enough for a reasonable acquisition time. To date, C_{60} provides the best single beam performance. It is expected that large cluster sources with high-brightness, suitable for high-resolution imaging, will be developed in the future.

In the present work, the possibility of enhancing the sensitivity of TOF-SIMS by analyzing a sample in a dual beam depth profiling mode has been tested directly on rat brain sections, which are the tissue samples commonly used for methodology studies in mass spectrometry imaging. 3D images have already been recorded on cells and tissues using a similar dual beam procedure but with C_{60} beams instead of argon clusters.[26,27] However, only fragment ions from cholesterol or lipid species were investigated in these two studies. We also study the optimization of the beam-1 and beam-2 ion dose conditions for maximum increases in sensitivity.

EXPERIMENTAL SECTION

Lipid standards. The lipids were purchased from Avanti Polar Lipids (Alabaster, AL, USA) and were all spotted onto a gold plate at a concentration of 1 mg/mL. Cholesterol (Chol), *N*-stearoyl-D-erythro-sphingosin (Cer C18:0), *N*-palmitoyl-D-sphingomyelin (SM 16:0), 1-palmitoyl-2-oleoyl-*sn*-glycerol (DG 16:0/18:1), glyceryl tripalmitate (TG 48:0), 1-palmitoyl-2-oleoyl-*sn*-glycero-3-phosphocholine (PC 16:0/18:1), and 1-palmitoyl-2-oleoyl-*sn*-glycero-3-phosphoethanolamine (PE 16:0/18:1) were dissolved in chloroform. α-Tocopherol (Vitamin E) was dissolved in ethanol at 10 mM, and the 1,2-dipalmitoyl-sn-glycero-3-phosphoinositol (PI 16:0) was dissolved in methanol/water/chloroform (45/5/50, V/V/V).

Rat brain Tissue sections. Rat brain sections (14 μm thick) were cut at −20 °C in a CM3050-S cryostat (Leica Microsystèmes SA, Nanterre, France) then deposited onto silicon wafers (2 in. diameter polished silicon wafers, ACM, Villiers-Saint-Frédéric, France) and dried under vacuum for a few minutes. The thickness of the dried rat brain sections was measured using a laser confocal microscope (Olympus LEXT OLS4000). The dried rat brain sections were found to be 1.2 ± 0.3 μm thick (less than 10% of the initial thickness), which is in agreement with Anthony et al.[28]

TOF-SIMS imaging. The TOF-SIMS imaging experiments were performed with a TOF-SIMS IV mass spectrometer (ION-TOF GmbH, Münster, Germany) located at the National Physical Laboratory (NPL, Teddington, United Kingdom) and with a TOF-SIMS IV (same manufacturer) located at the Institut de Chimie des Substances Naturelles (CNRS, Gif-sur-Yvette, France). The first instrument is fitted

dx.doi.org/10.1021/ac4009513 | Anal. Chem. 2013, 85, 7745−7752

with two types of ion sources, also manufactured by ION-TOF GmbH. One primary ion source is a liquid metal ion gun (LMIG) which delivers bismuth cluster ions (Bi_3^+ selected with a 25 keV kinetic energy). This spectrometer is able to perform dual beam depth profiling, thanks to an argon cluster ion source. Ar_n^+ ions (with n = 500 to 2000), with a kinetic energy between 5 and 20 keV, hit the sample surface with an angle of incidence of 45°. Positive and negative ion images were recorded with the same parameters: irradiation with Ar sputtering beam, with a current of 1 or 2 nA, during 4 s, over an area of 500 μm × 500 μm (the Ar_n^+ beam size is ∼50 μm wide, with a Gaussian-like profile), followed by a surface analysis with Bi_3^+ primary ions during 3.3 s over an area of 150 μm × 150 μm inside and at the center of the previously sputtered area. The internal mass calibration was performed using low mass ions always present: H^+, C^+, CH^+, CH_2^+, CH_3^+, CH_4^+, $C_2H_3^+$, and $C_2H_5^+$ in the positive ion mode and H^-, C^-, CH^-, C_2^-, C_3^-, and C_4H^- in the negative ion mode. For the analyses of tissue sample sections, as the surface of the sample is not fully conductive, the potential of the surface is not at ground potential but slightly above. In order to maintain high mass resolution and high transmission, the analyzer has been tuned in this respect prior to each measurement.[29] The instrument located at CNRS was used for the study of the influence of cholesterol on the signal intensity of the lipids. Spectra were acquired over a 300 μm × 300 μm area, with 64 × 64 pixels and a Bi_3^+ PID (kinetic energy 25 keV) of 5 × 10^{10} ions/cm^2. All intensities reported are corrected for Poisson counting statistics.

The secondary ion emission yields, Y, were calculated in the case of the lipid standards analyses and are defined as the ratio of the area of the peak of interest (or the intensity) over the number of primary ions impinging the surface during the acquisition.[3] The name of the compound or the m/z value of the corresponding ion, the maximum of counts in a pixel (MC), and the total counts (TC) are shown below each image. The color scales correspond to the interval [0,MC].

RESULTS AND DISCUSSION

The study was focused on the capacity of the argon source to be used to sputter the surface, allowing then a depth profiling analysis of a biological sample, and a consequent increase of the sensitivity for tissue analysis. Rat brain sections were studied by dual beam profiling, alternating a cluster bismuth ion beam to analyze the sample surface with an argon cluster ion beam to sputter and clean the surface before a new analysis. The parameters of the selected argon cluster beam were a cluster size of 1500 atoms ($M/\Delta M \sim 5$) and a kinetic energy of 10 keV, in order to find a compromise between the analysis time and the number of data points. It has to be noted that the gas cluster ion source generates a broad cluster distribution, ranging from several hundred atoms to several thousand atoms per cluster. The selected value of 1500 atoms is only the mean value of a broad distribution selected with a resolution of ∼5. Although the effective cluster size is not exactly 1500, because of the asymmetry of the cluster size distribution,[30] the nominal value of 1500 is used for simplicity. The aim of the experiment was to sputter the tissue until reaching the underlying silicon wafer, in order to estimate the sputtered thickness, and to correlate it with the argon sputtering rate. Meanwhile, this experiment also allows one to evaluate the sensitivity enhancement by the use of this dual beam depth profiling method. We adapted the kinetic energy of the bismuth cluster source, set at 25 keV, to be similar to what is usually applied in our imaging protocol for biological samples.[31−33] All the parameters are summarized in the Table S-1, Supporting Information.

The sizes of the sputtered and analyzed areas were described in the Experimental Section. The experiment was performed using a total primary ion dose (PID) of 1.7 × 10^{13} ions/cm^2 for the bismuth ion beam and 1.57 × 10^{16} ions/cm^2 for the argon ion beam. As a control, an ion image was first recorded according to the usual surface analysis conditions (PID = 3 × 10^{11} ions/cm^2 under static conditions) on the same location and just before the dual beam profiling. Each positive and negative ion mode analysis was performed on a different tissue sample in order to prevent any disturbance of an experiment by the previous one, such as charge effect, any possible modification of the tissue section, or surface contamination by sputtered material. The images and spectra were divided into several parts acquired after each 10^{12} bismuth ions/cm^2, each corresponding to 50 scans. This way of analyzing the data allows us to study the images and the intensity of some peaks for each part or for the sum of several parts, in order to check the effect of the depth profiling on the sensitivity.

To confirm the amount of sample which was sputtered over the analysis, we checked the profile (intensity as a function of PID) of silicon and controlled the optical image using the video camera of the instrument. After the analysis, optical pictures were recorded with a microscope and an example is shown in Figure 1. The first picture (Figure 1a) shows the entire rat brain section before the analysis, while the second one (Figure 1b) shows the same section after analysis. The analyzed area is shown at the bottom of the second picture, corresponding to the black square at the center of the sputtered area, inside the cerebellum. The sputtering process is evidenced since the picture shows a gray square corresponding to silicon which is no longer covered by the tissue section. However, it does not look uniform, since some parts of the sample are still present. Figure 2 presents the assessment within each part or the profile versus the PID of bismuth and argon in the positive (Figure 2a) and negative (Figure 2b) ion modes, respectively. Over the whole analysis, it was possible to isolate a positive ion spectrum corresponding to each fraction of 10^{12} ions/cm^2 of Bi_3^+ ions and we plotted the intensity of each ion peak. Each part corresponding to an interval of 10^{12} ions/cm^2 of Bi_3^+ is numerated on the Figure 2a; part 1 corresponds to the interval between 0 and 1 × 10^{12}, part 2 represents the interval between 1 and 2 × 10^{12} ions/cm^2, and so on. Figure 2a is therefore the variation of some peak intensities within each part of 10^{12} ions/cm^2 (Bi_3^+). The silicon ion, m/z 27.9, intensity is represented by the blue squares. It presents a sigmoidal behavior in which the inflection point was attributed to the transition between the sample and the underlying silicon. This provides an approximate depth scale, in percentage, written at the top of this figure. Since the tissue thickness under vacuum is much lower than the original 14 μm thickness due to water evaporation, it is not possible to write an absolute eroded thickness. That is why the sputtered thickness is scaled in percentage. The other ion intensities decrease in the same way when the silicon ion signal begins to increase from 1.4 × 10^{13} ions/cm^2 bismuth ions. The potassium ion signal at m/z 38.9 does not present any variation. This ion is saturated and is detected all over the whole volume analyzed. In the case of m/z 184, corresponding to the head of the phosphatidyl group, a characteristic fragment of phosphocholines and sphingomye-

dx.doi.org/10.1021/ac4009513 | Anal. Chem. 2013, 85, 7745−7752

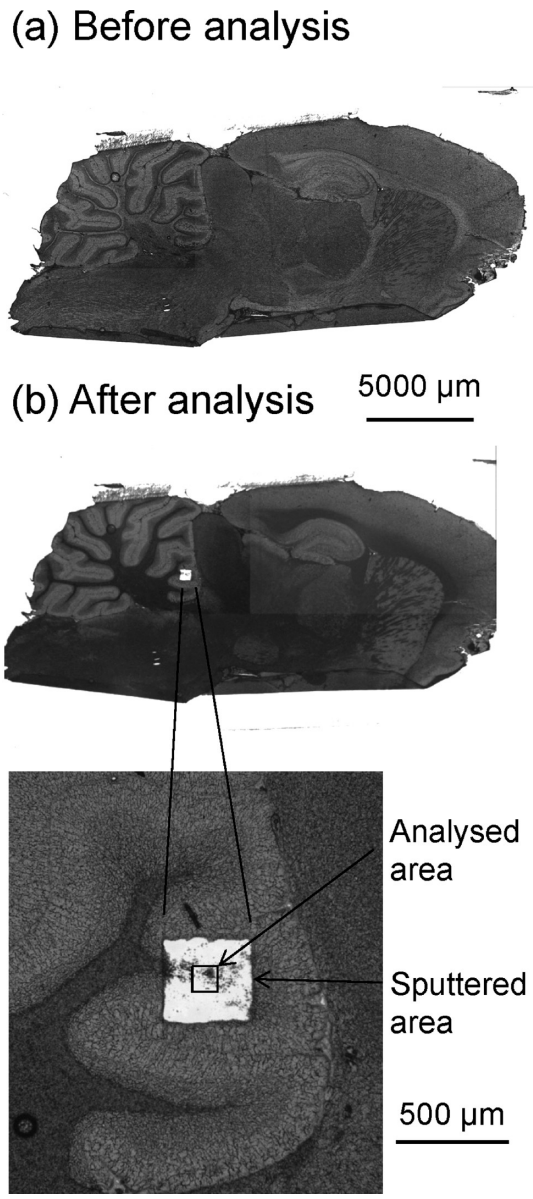

Figure 1. Optical images of the rat brain slices before (a) and after (b) dual beam profiling. The area analyzed was zoomed, and the sputtered and analyzed areas were highlighted.

lins, and all the phosphocholines PCs, between m/z 730 and 805 (empty and filled circles), their signals stay constant all along the sample thickness analyzed. The m/z 224 ion intensity (top triangles) displays an analogous behavior as the group of PCs. This could be expected as this ion is a specific fragment of the phosphocholine species. The variation for the Vitamin E at m/z 430 is similar to the others with the lowest values. All these ion species have similar behavior, and especially along the whole sample thickness, their signal intensities remain constant. The case of cholesterol ions at m/z 369 and 385, corresponding to $[\text{cholesterol} + \text{H} - \text{H}_2\text{O}]^+$ and $[\text{cholesterol} - \text{H}]^+$, respectively, is atypical. Their intensity variations are strongly decreasing at the beginning of the irradiation (until 6×10^{12} ions/cm^2 bismuth ions) and in a second step show comparable variations and values as the Vitamin E (i.e., a plateau and then a slight decrease). The presence of a decrease in signal intensity for all the selected peaks is explained by the irregular aspect of the sample surface. The sputtering process is homogeneous, but

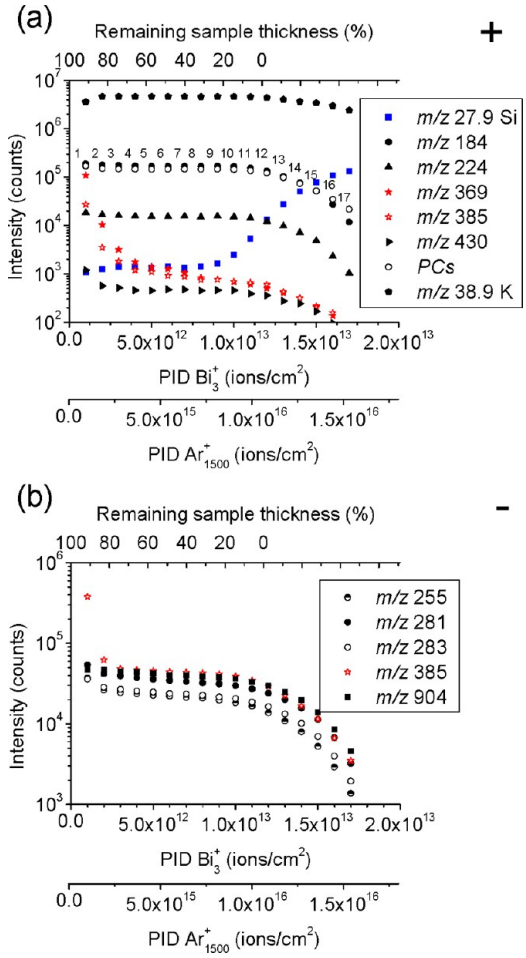

Figure 2. Intensities of several ions as a function of the analysis (Bi_3^+) and sputtering (Ar_{1500}^+) ion doses densities. (a) Positive ion mode; (b) negative ion mode. The error bars, corresponding to $(N)^{1/2}$ (with N the intensity in number of counts) are two small to be reported on the graphic.

the surface is not flat, so when reaching the silicon, some particles of sample may still be present and continue to give signal. The analysis of the tissue section in the negative ion mode is shown in Figure 2b. The variations of the intensities of some ions detected in the negative ion mode are shown as a function of the PID of bismuth and argon as well as versus the remaining sample thickness previously calibrated in percentage (top of the plot). A similar behavior is observed for all the curves, except for the cholesterol (open stars). The main difference between the various ions, fatty acids m/z 255 (C16:0), m/z 281 (C18:1), and m/z 283 (C18:0), or the sum of the entire isotopic pattern of the hydroxylated sulfatide ST42:2-OH at m/z 904 lies in their relative intensities, which are however relatively close to each other. The cholesterol ion $[\text{cholesterol} - \text{H}]^-$, at m/z 385, shows the same atypical behavior as in positive ion mode: a strong decrease in the first 3 $\times 10^{12}$ ions/cm^2 of bismuth followed by a variation similar to the other ions. Before investigating the increase of the sensitivity, the particular behavior of the cholesterol needs to be specifically described.

Atypical Behavior of Cholesterol. The unique behavior of this compound was investigated in detail, particularly at the beginning of the sample irradiation. The corresponding profile is shown in Figure 3a. The intensity of the $[\text{cholesterol} - \text{H}]^+$

dx.doi.org/10.1021/ac4009513 | Anal. Chem. 2013, 85, 7745−7752

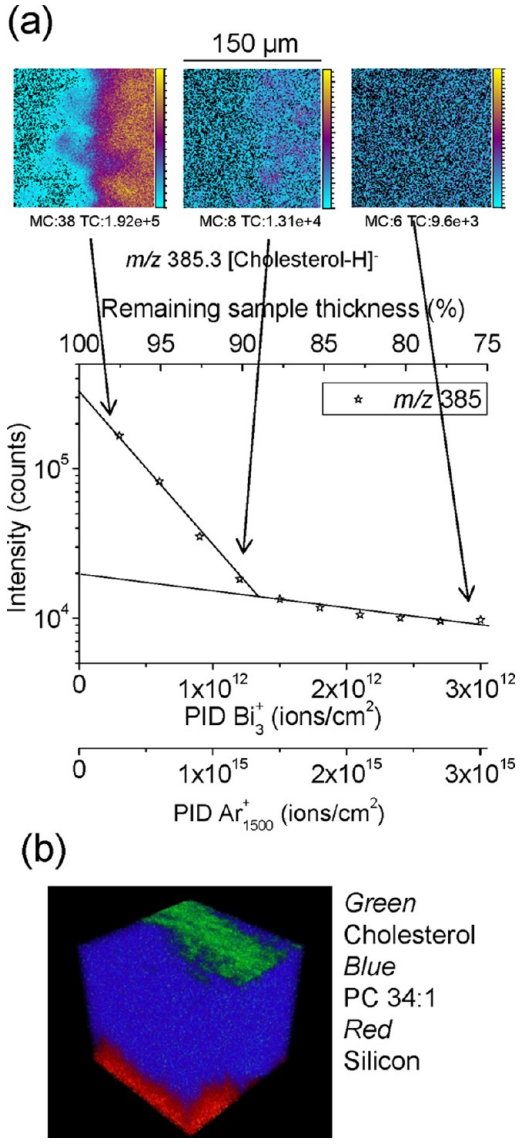

Figure 3. (a) Images of cholesterol ion at different stages during the dual beam depth profiling of a rat brain tissue section and cholesterol ion intensity as a function of the analysis (Bi_3^+) and sputtering (Ar_{1500}^+) ion doses densities. (b) 3D reconstruction of the sputtered volume, exemplified with 3 secondary ions over the whole thickness of the rat brain section.

ion at m/z 385 was plotted as a function of the PID of argon and bismuth ions, as well as of the remaining sample thickness, between 100 and 75% (top scale). However, in the plot of the Figure 3, each point corresponds to an interval of 10^{11} Bi_3^+ ions/cm^2 to obtain a zoom of the data from the Figure 2. The log of intensity decreases linearly as a function of the dose, but with two different lines having two different slopes, the first being larger than the second. This change of slope may correspond to the limit of the presence of cholesterol at and beneath the surface and can be evaluated to ~10% of the sample thickness. At the top of Figure 3a are shown cholesterol ion images extracted from the data sets, each with bismuth intervals of 10^{11} ions and after PID of 3×10^{11} and 1.2 and 3×10^{12} ions/cm^2, respectively. Between the first and the second image, the MC and TC values dramatically decreased, from a factor of 5 in the case of MC and of 15 for TC, and the initial tissue structure is not anymore distinguishable. The third image showed almost similar results as the second one, confirming that the cholesterol was mainly located close to the sample surface. Surface Lab 6.2 software allows the visualization of the data in a 3-dimensional way. We choose, for this representation, a three color overlay, with silicon in red, only detected at the end of the experiment, a lipid having a constant intensity, such as a PC, here PC 34:1 at m/z 760.6, in blue, and cholesterol, in green. This representation could have been done with various types of lipids, instead of the PC chosen, as they all show constant intensity over the whole sample thickness. The corresponding reconstructed volume is shown in Figure 3b. Cholesterol appears to be located only at the top of the cube, clearly illustrating the above results, here equivalent to almost 1.5−2 μm thickness of the original section, while the PC chosen (in blue) covers almost the entire thickness of the sample. The silicon signal is emerging from the bottom of the cube, due to the support, but is not homogeneous. This is likely because the sample surface is rough and not flat, and the software does not make the volume reconstruction from the bottom surface but from the top as viewed by beam-1. This particular localization of cholesterol is in agreement with the work of Jones et al.,[27] as well as with the two previous studies made by Sjövall et al. and by Debois et al., who both hypothesized that cholesterol, and other ion species, could concentrate close to the surface when maintaining a tissue section under vacuum and at room temperature.[34,35] This will be discussed later.

Toward an Increase of Sensitivity for Tissue Imaging. As already shown in Figure 2, the intensities of the ion peaks of lipids or lipid fragments are quite constant during the sputtering of the whole thickness of the sample. This means that a dual beam depth profiling is efficient in this kind of tissue, similar to that already demonstrated in model samples like amino-acid or Irganox stacks.[21,22] It may also be possible to sum over a certain depth of the sample the signal of any ion, corresponding to several layers, in order to obtain better information of the chemical composition of the tissue sample. This was done for example, for the sulfatide ion $[ST42:2\text{-}H]^-$ at m/z 888.6 in the negative ion mode (Figure S-1, Supporting Information). First, the surface image of this ion, obtained when analyzing it under usual bismuth PID of 5×10^{11} ions/cm^2, is shown as the reference (in the red square, Figure S-1a, Supporting Information). The MC value is at 8, and the TC value is about 1.6×10^4, allowing the distinction of the biological substructure. Second, in the two following images of the part 1 and part 2, each obtained with 1×10^{12} ions/cm^2 of Bi_3^+, the signal is almost constant with MC values of 8 and 9, respectively, and also equivalent TC values (around $1.6\text{−}1.7 \times 10^4$). The localization of this ion appears different than in the case of the surface image, and this will be developed later on. However, if these two images are added, the resulting image presents larger MC and TC values. As expected for images limited by Poisson counting statistics, the MC value for part 1 added to part 2 is $(MC_1^2 + MC_2^2)^{1/2}$, a similar relationship would occur if the substance is randomly distributed in the sample. The TC value for the added image, is of course, approximately twice the individual TC values since intensities remain approximately constant. The improved signal-to-noise clearly gives localization of the species (Figure S-1b, Supporting Information) even without the shift correction noted earlier. The same addition process can be performed on the rest of the thickness of the tissue sample in order to increase in a large way the sensitivity for this ion (Figure S-1c, Supporting

dx.doi.org/10.1021/ac4009513 | Anal. Chem. 2013, 85, 7745−7752

Information). The image acquired from the sum of the signal between 2 and 11 × 10^{12} ions/cm^2 (or from part 3 until part 12 as explained in Figure 2), thus corresponding to 9 × 10^{12} ions/cm^2 and to almost the whole thickness of the sample section, is now obtained with a MC value of 35 and TC value at 1.38 × 10^5, which means an enhancement of almost 4 times in the case of the MC value (slightly higher than the expected $(12)^{1/2}$) and almost 9 times in the case of the TC value, in comparison to the surface ion image (slightly less than the expected 12, most likely owing to a declining intensity). Other examples of enhancement of the intensities of lipids, until 50 times more for the TC value, can be cited over the whole m/z range, in positive and negative ion modes, with other combinations of Ar ion beam (cluster size, energy, and relative Ar and Bi PID) as shown in Figure 4. The ion images obtained at the surface sample in the case of the PC 34:1 in the positive ion mode, as molecular ion or as a PC fragment at m/z 224, and in the case of the fatty acid C18:1 in the negative ion mode are shown in Figure 4a,b,c, respectively. The MC and TC values have to be compared to the images obtained over the whole sample thickness of these three ions (presented on the right panel) to evaluate the increase of the sensitivity. In terms of MC values, the increase is about 5, 47, and 16 times more, but in the case of the TC values, the fatty acid signal is increased by a factor of 25, the PC molecular ion signal is increased 50 times, and the PC fragment signal (m/z 224) is increased by a factor of 120. Thus, this dual beam depth profiling allows a strong increase of sensitivity for a lot of various lipids species, in positive and negative ion modes.

Nevertheless, an apparent change in the detected localization of the compound is noticeable. Indeed, the localization of the ST 42:2 at the surface, with a Bi_3^+ PID of 5 × 10^{11} ions/cm^2 (on the left part of the image, Figure S-1a, Supporting Information), is totally different than that observed with the analyses done deeper in the sample, when increasing the PID (mainly on the right part of the image, Figure S-1c, Supporting Information). This surprising behavior can potentially have two different explanations, one of them coming from a different lipid composition between the surface layer and the deeper layers. This first hypothesis was already formulated by Debois et al. when testing a dual beam depth profiling in a tissue sample using fullerenes instead of argon clusters to sputter the sample. They observed that some ion species appeared to be concentrated in the first layers of the samples.[35] According to previous analyses made by Sjövall et al.[34] as a function of the sample temperature, they attributed it to a migration toward the sample surface during the unfreezing of the sample under vacuum. Another hypothesis could be due to the amount of cholesterol, present only at the surface. Sulfatide ion species can be present everywhere in the sample section, but at the surface, its signal may be suppressed by cholesterol. When the cholesterol disappears, at a depth of ∼1.5−2 μm, the signal of the studied ion can be detected. This is the so-called "matrix effect", i.e., the enhancement or the decrease (here a decrease) of some ion species due the chemical microenvironment.[25,36] In order to test these hypotheses, the secondary ionization yield of several lipids was evaluated for pure compounds or mixed with cholesterol. Solutions were prepared at 1 mg/mL, and 0.5 μL was deposited onto a gold plate, without or with the addition of 0.5 μL of a cholesterol solution (1 mg/mL). The secondary ion yields were measured for some ions in positive and negative ion modes. The variation is obvious when looking at the yield value measured for each lipid ion in the presence of cholesterol

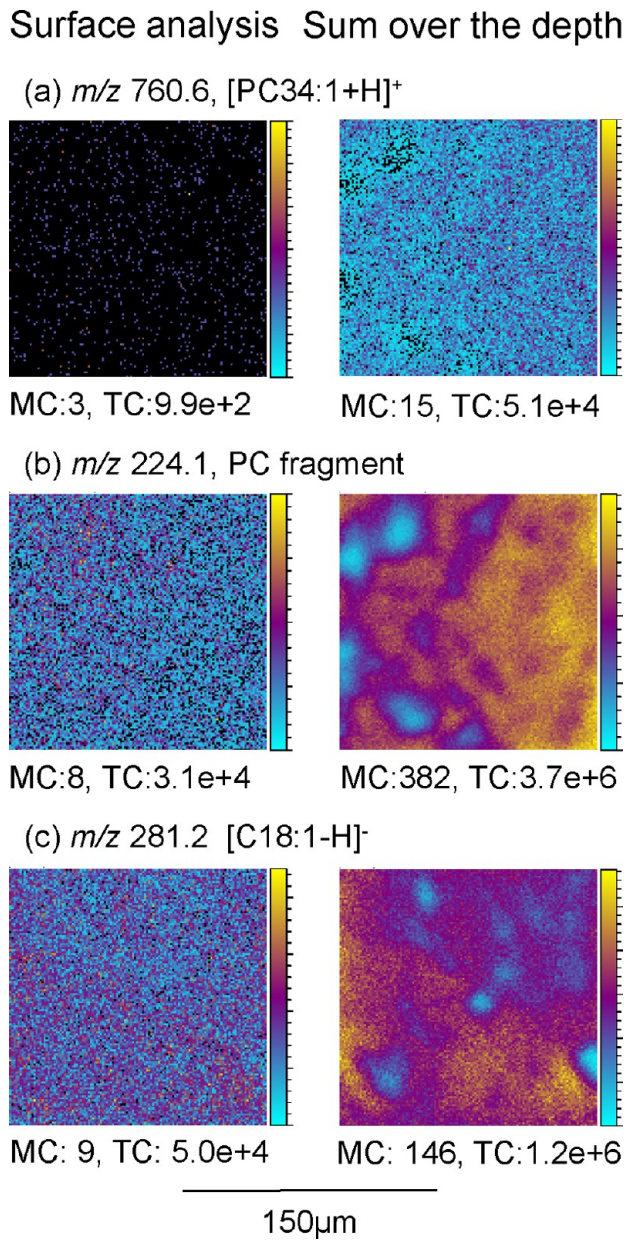

Figure 4. (a) Images of the PC 34:1 ion at m/z 760.6 (b) and images of a PC fragment ion ($C_8H_{19}NO_4P$) at m/z 224.1 in the positive ion mode. (c) Images of the fatty acid C18:1 ion at m/z 281.2 in the negative ion mode obtained at the sample surface and obtained from the sum over the whole sample thickness (right panel).

(Table S-2, Supporting Information). The ion at m/z 687 ($[SM34:1-H]^-$, sphingomyelin fragment) in the negative ion mode is the only one for which the yield value is slightly larger in the presence of cholesterol. For all the other lipids, the yields are slightly lower, like in the cases of sulfatide 42:2, $[M - H]^-$ ion, Ceramide, $[M + H]^+$, and $[M + Na]^+$ ions or 3 times lower such as for the Vitamin E in the positive ion mode or for the TG 48:0 in the positive ($[M + Na]^+$) or in the negative ($[M - H]^-$) ion modes (ratio at 3.2 and 2.3, respectively) or even 9 to 10 times smaller in the case of the PE 34:1 in the positive and negative ion modes. This phenomenon can thus partially explain the difference in the apparent localization of some ions when going deeper into the sample, as after 2 μm, since the cholesterol has almost entirely disappeared and thus does not

dx.doi.org/10.1021/ac4009513 | Anal. Chem. 2013, 85, 7745−7752

reduce the ionization efficiency. However, there is no clear explanation why cholesterol is concentrated under vacuum at or close to the surface of the sample or why the presence of cholesterol can have an influence on desorption or ionization of neighboring compounds. The migration of the cholesterol inside the lipid bilayer is known and possible, but the exact phenomenon which happens under vacuum on tissue sections is not yet well-defined.

Optimization of the Relative Beam-1 Dose for Increased Signal Enhancement. As discussed in the introduction, the sensitivity enhancement that can be achieved by accumulating secondary ion intensity from the entire depth of a sample depends on the ratio of the two ion beam doses as well as the operation mode. In the experiments above, the Bi_3 ion beam imaged the surface using one pulse per pixel between removing material with argon cluster ions for 4 s. The PID of a single Bi_3^+ scan was 2.0×10^{10} ions/cm^2 which is well within the static SIMS regime. While the conventional definition of a static limit does not apply to the dynamic dual beam experiment here, the comparison indicates that the PID can be increased to further enhance sensitivity. To assess this potential, a series of measurements with different numbers of Bi_3^+ pulses per pixel between sputtering cycles were carried out. This effectiveness of this approach is indicated by Muramoto et al. in a study of the effects of beam-1 dose on the quality of depth profiles obtained with C_{60} for a trehalose film.[37] In that study, they clearly showed that the depth profile quality degraded substantially as the relative dose of beam-1 increased when using monatomic Bi^+ ions, while for Bi_3^+ primary ions the effects on intensity were not too severe although the depth resolution degraded. In this study, we are concerned with improving ultimate analytical signal, which also improves useful lateral resolution,[9,38] rather than the depth-resolution.

Prior to the measurements, the tissue sample was sputtered with argon clusters to reach the homogeneous part of the sample beneath the cholesterol-rich surface. The m/z 184 profile, corresponding to the head of the phosphatidyl group, was then acquired using between 1 and 80 Bi_3^+ pulses per pixel in-between 4 s cycles of Ar_{1500}^+ sputtering (conditions as above), corresponding to a Bi_3^+ dose of $N \times 1.7 \times 10^{10}$ ions/cm^2, where N is the number of pulses per pixel, and an Ar_{1500}^+ dose of 1.5×10^{13} ions/cm^2 per cycle. For each dose ratio condition, 20–40 sputter-analysis cycles were acquired.

In all cases, the m/z 184 ion intensity per analysis cycle was constant or reached a constant level, the steady state intensity, within a few analysis cycles (data not shown). Figure 5 shows the m/z 184 ion steady state intensity divided by the total ion dose (Ar_{1500} + Bi_3) as a function of the dose ratio. Here, we assume that the sputtering yield volumes for Ar_{1500} and Bi_3 are approximately similar so that the normalization is equivalent to the amount of material consumed. Figure 5 shows the effect of the ion dose ratio between beam-1 and beam-2 on the maximum sensitivity gain achievable if all the material is consumed. It is clear that the sensitivity gain can be significantly enhanced by increasing the Bi_3^+ dose relative to the Ar_{1500}^+ dose. The enhancement is particularly strong for the first factor 10–20 increase in Bi_3^+ dose from the 1 pulse per pixel condition and drops off at higher dose ratio values as Bi_3^+ damage plays an increasingly larger role. If the dose ratio was to be increased even more, the intensity sensitivity gain would decrease. The optimum is in this case seen for a dose ratio between 0.05 and 0.09 for which the signal is nearly 14 times higher than for the 1 pulse per pixel condition. The optimal dose ratio is not generic but depends on the sputtering yield of the beam-2 ions as well as the beam-2 ion dose per sputter cycle. The latter is because the beam-2 dose required clean up of the damage caused by beam-1 which is not linearly correlated with the beam-1 dose. Naturally, the further enhanced sensitivity comes at a price of increased experiment time. To collect ions from the entire depth of the tissue slice with the conditions that give the highest accumulated secondary ion signal will take approximately 15 times longer than the 1 pulse per pixel condition.

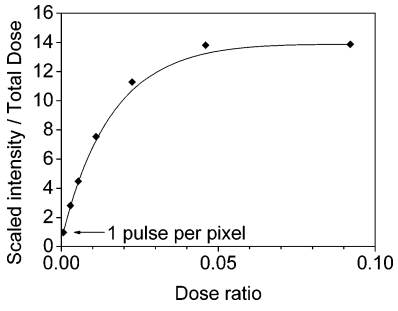

Figure 5. The m/z 184 ion steady state intensity divided by the total dose as a function of beam-1 (Bi_3^+) to beam-2 (Ar_{1500}^+) dose ratio. The intensity/dose values have been normalized to the value for the 1 pulse per pixel condition used in previous measurements. The solid line is to guide the eye.

CONCLUSION

Argon cluster beams have been used to sputter depth profile through an entire rat brain tissue section having an initial thickness of 14 μm, in order to test the possibility of depth profiling into a real biological sample. We show that the tissue dehydrates in vacuum to approximately 10% of the initial thickness. A two beam depth profiling experiment was performed until reaching the underlying silicon wafer. The signal of most of the lipid ion species was constant over the entire thickness of the sample, proving that no or very little sample damage occurred. However, the cholesterol behaved differently, appearing to be mainly concentrated at or just beneath the surface of the tissue sample, in a depth estimated to 10% of the sample thickness. This evaluation of the localization of the cholesterol was illustrated by a 3-dimensional representation. Cholesterol also generated a strong surface matrix effect on the ionization of several other lipid ions. Finally, it could be shown that the sensitivity for a single lipid ion species can be greatly enhanced thanks to the dual beam process using the argon source. The argon clusters source positively shows its capacities in analyzing organic standards, allowing the dual beam depth profiling of biological tissue samples, together with possible enhancements of the sensitivity by a factor of 1 hundred or more. Furthermore, we show that the enhancement may be further increased by increasing the ratio of the beam-1 (analysis) to beam-2 (sputter) dose by up to a factor of 14 at the experimental cost of a similar increase in analysis time and poor depth resolution, which could be an issue for some studies.

ASSOCIATED CONTENT

Supporting Information

Additional information as noted in text. This material is available free of charge via the Internet at http://pubs.acs.org.

dx.doi.org/10.1021/ac4009513 | Anal. Chem. 2013, 85, 7745–7752

AUTHOR INFORMATION

Corresponding Author

*Phone: +33 169 824 575. E-mail: Alain.Brunelle@cnrs.fr.

Notes

The authors declare no competing financial interest.

ACKNOWLEDGMENTS

Sabine De La Porte is gratefully acknowledged for her help in graciously providing the rat brains. This work and the postdoctoral fellowship position of C.B. are supported by the Agence Nationale de la Recherche (Grant ANR-2010-BLAN-0805-01-MASS-IMAGE). This work was partially supported by the National Physical Laboratory's Strategic Research Programme (Project SR116301 – NiCE-MSI).

REFERENCES

(1) Sjövall, P.; Lausmaa, J.; Johansson, B. *Anal. Chem.* **2004**, *76*, 4271–4278.

(2) Touboul, D.; Halgand, F.; Brunelle, A.; Kersting, R.; Tallarek, E.; Hagenhoff, B.; Laprévote, O. *Anal. Chem.* **2004**, *76*, 1550–1559.

(3) Touboul, D.; Kollmer, F.; Niehuis, E.; Brunelle, A.; Laprévote, O. *J. Am. Soc. Mass Spectrom.* **2005**, *16*, 1608–1618.

(4) Weibel, D.; Wong, S.; Lockyer, N.; Blenkinsopp, P.; Hill, R.; Vickerman, J. C. *Anal. Chem.* **2003**, *75*, 1754–1764.

(5) Bolbach, G.; Viari, A.; Galera, R.; Brunot, A.; Blais, J. C. *Int. J. Mass Spectrom. Ion Processes* **1992**, *112*, 93–100.

(6) Benguerba, M.; Brunelle, A.; Della-Negra, S.; Depauw, J.; Joret, H.; Le Beyec, Y.; Blain, M. G.; Schweikert, E. A; Ben Assayag, G.; Sudraud, P. *Nucl. Instrum. Methods Phys. Res., Sect. B* **1991**, *62*, 8–22.

(7) Brunelle, A.; Della-Negra, S.; Depauw, J.; Jacquet, D.; Le Beyec, Y.; Pautrat, M.; Baudin, K.; Andersen, H. H. *Phys. Rev. A* **2001**, *63* (022902), 1–10.

(8) Fletcher, J. S.; Vickerman, J. C. *Anal. Chem.* **2013**, *85*, 610–639.

(9) Vickerman, J. C. TOF-SIMS – an overview. In *ToF-SIMS - Surface Analysis by Mass Spectrometry*; Vickerman, J. C., Briggs, D., Eds.; Surface Spectra and IM Publications: Manchester and Chichester, 2001; pp 1–40.

(10) Gilmore, I. S. Role of operating conditions in ToF-SIMS. In *TOF-SIMS Surface Analysis by Mass Spectrometry*, second ed.; Vickerman, J. C., Briggs, D., Eds.; Surface Spectra and IM Publications: Manchester and Chichester, in press.

(11) Lee, J. L. S.; Ninomiya, S.; Matsuo, J.; Gilmore, I. S.; Seah, M. P.; Shard, A. G. *Anal. Chem.* **2010**, *82*, 98–105.

(12) Matsuo, J.; Okubo, C.; Seki, T.; Aoki, T.; Toyoda, N.; Yamada, I. *Nucl. Instrum. Methods Phys. Res., Sect. B* **2004**, *219–220*, 463–467.

(13) Ninomiya, S.; Nakata, Y.; Ichiki, K.; Seki, T.; Aoki, T.; Matsuo, J. *Nucl. Instrum. Methods Phys. Res., Sect. B* **2007**, *256*, 493–496.

(14) Ninomiya, S.; Ichiki, K.; Yamada, H.; Nakata, Y.; Seki, T.; Aoki, T.; Matsuo, J. *Rapid Commun. Mass Spectrom.* **2009**, *23*, 1601–1606.

(15) Moritani, K.; Houzumi, S.; Takeshima, K.; Toyoda, N.; Mochiji, K. J. *Phys. Chem. C* **2008**, *112*, 11357–11362.

(16) Moritani, K.; Hashinokuchi, M.; Nakagawa, J.; Kashawagi, T.; Toyoda, N.; Mochiji, K. *Appl. Surf. Sci.* **2008**, *255*, 948–950.

(17) Mochiji, K.; Hashinokuchi, M.; Moritani, K.; Toyoda, N. *Rapid Commun. Mass Spectrom.* **2009**, *23*, 648–652.

(18) Tanaka, M.; Moritani, K.; Hirota, T.; Toyoda, N.; Yamada, I.; Inui, N.; Mochiji, K. *Rapid Commun. Mass Spectrom.* **2010**, *24*, 1405–1410.

(19) Chen, Y. Y.; Yu, B. Y.; Wang, W. B.; Hsu, M. F.; Lin, W. C.; Lin, Y. C.; Jou, J. H.; Shyue, J. J. *Anal. Chem.* **2008**, *80*, 510–505.

(20) Lee, J. L. S.; Seah, M. P.; Gilmore, I. S. *Appl. Surf. Sci.* **2008**, *255*, 934–937.

(21) Shard, A. G.; Havelund, R.; Seah, M. P.; Spencer, S. J.; Gilmore, I. S.; Winograd, N.; Mao, D.; Miyayama, T.; Niehuis, E.; Rading, D.; Moellers, R. *Anal. Chem.* **2012**, *84*, 7865–7873.

(22) Wehbe, N.; Tabarrant, T.; Brison, J.; Mouhib, T.; Delcorte, A.; Bertrand, P.; Moellers, R.; Niehuis, E.; Houssiau, L. *Surf. Interface Anal.* **2013**, *45*, 178–180.

(23) Tempez, A.; Schultz, J. A.; Della-Negra, S.; Depauw, J.; Jacquet, D.; Novikov, A.; Le Beyec, Y.; Pautrat, M.; Caroff, M.; Ugarov, M.; Bensaoula, H.; Gonin, M.; Fuhrer, K.; Woods, A. *Rapid Commun. Mass Spectrom.* **2004**, *18*, 371–376.

(24) Ziegler, J. F.; Biersack, J. P.; Littmark, U. *The Stopping and Ranges of Ions in Solids*; Pergamon Press: New York, 1985; SRIM 2013, www.srim.org.

(25) Muramoto, S.; Brison, J.; Castner, D. G. *Anal. Chem.* **2012**, *84*, 365–372.

(26) Robinson, M. A.; Graham, D. J.; Castner, D. G. *Anal. Chem.* **2012**, *84*, 4880–4885.

(27) Jones, E. A.; Lockyer, N. P.; Vickerman, J. C. *Anal. Chem.* **2008**, *80*, 2125–2132.

(28) Anthony, A.; Clurso, G. J.; Bocan, T. M. A.; Doebler, J. A. *Histochem. J.* **1984**, *16*, 61–70.

(29) Seyer, A.; Einhorn, J.; Brunelle, A.; Laprévote, O. *Anal. Chem.* **2010**, *82*, 2326–2333.

(30) Matsuo, J.; Ninomiya, S.; Nakata, Y.; Ichiki, K.; Aoki, T.; Seki, T. *Nucl. Instrum. Methods Phys. Res., Sect. B* **2007**, *257*, 627–631.

(31) Brunelle, A.; Touboul, D.; Laprévote, O. *J. Mass Spectrom.* **2005**, *40*, 985–999.

(32) Touboul, D.; Roy, S.; Germain, D. P.; Chaminade, P.; Brunelle, A.; Laprévote, O. *Int. J. Mass Spectrom.* **2007**, *260*, 158–165.

(33) Benabdellah, F.; Seyer, A.; Quinton, L.; Touboul, D.; Brunelle, A.; Laprévote, O. *Anal. Bioanal. Chem.* **2010**, *396*, 151–162.

(34) Sjövall, P.; Johansson, B.; Lausmaa, J. *Appl. Surf. Sci.* **2006**, *252*, 6966–6974.

(35) Debois, D.; Brunelle, A.; Laprévote, O. *Int. J. Mass Spectrom.* **2007**, *260*, 115–120.

(36) Jones, E. A.; Lockyer, N. P.; Vickerman, J. C. *Int. J. Mass Spectrom.* **2007**, *260*, 146–157.

(37) Muramoto, S.; Brison, J.; Castner, D. G. *Surf. Interface Anal.* **2011**, *43*, 58–61.

(38) Kollmer, F. *Appl. Surf. Sci.* **2004**, *231*, 153–158.